Rare Metal Materials and Engineering
Volume 55, Issue 10, October 2026
Available online at www.rmme.ac.cn

Science Press

Cite this article as: Zhang Pengtao, Cheng Xiaole, Ren Xijun, et al. Novel Constant-Strain-Rate Backward Extrusion for AZ91 Magnesium Alloy[J]. Rare Metal Materials and Engineering, 2026, 55(10): 2491-2500.
DOI: https://doi.org/10.12442/j.issn.1002-185X.20250389.

ARTICLE

Novel Constant-Strain-Rate Backward Extrusion for AZ91 Magnesium Alloy

Zhang Pengtao[1], Cheng Xiaole[1], Ren Xijun[2], Zhang Min[1], Bian Chenghao[1], Sun Jian[1], Zhao Xiaohui[1], Su Zhenhua[3]

[1] School of Mechanical and Electrical Engineering, Xi'an Polytechnic University, Xi'an 710048, China; [2] Xi'an Xicai Sanchuan Intelligent Manufacturing Co., Ltd, Xi'an 710600, China; [3] China National Heavy Machinery Research Institute Co., Ltd, Xi'an 710018, China

Abstract: To overcome the limitations of poor room-temperature ductility and significant anisotropy in AZ91 magnesium alloy, a constant-strain-rate backward extrusion (CSR-BE) process was introduced to enhance deformation homogeneity through synergistic regulation of die curvature and strain rate. The methodology employs axisymmetric slip-line theory, combined with volume constancy principles, to derive a die profile equation that enables precise control of strain rates throughout deformation. Comprehensive DEFORM-3D simulations reveal that CSR-BE achieves a 9.3% reduction in extrusion force compared to conventional backward extrusion, accompanied by substantial improvements in deformation uniformity: a 99.96% decrease in flow velocity variance, an 85.2% reduction in stress field variation, and an 81.6% mitigation of temperature distribution fluctuations. Mechanistic analysis demonstrates that the optimized die geometry shifts the material flow dominance from radial shear to axial stretching, characterized by a decrease in the slip-line orientation angle from 36.27° at the inlet to 11.3° at the outlet. The engineered hydrostatic pressure gradient effectively alleviates localized stress concentrations, eliminates friction-induced dead zones, and suppresses strain-rate variations. Quantitative stress and flow-rate calculations confirm that this approach fundamentally addresses the microstructural heterogeneity inherent to traditional extrusion methods. CSR-BE process establishes a theoretically grounded manufacturing strategy for producing high-performance magnesium alloy rods with enhanced isotropy, demonstrating significant potential for industrial-scale applications through its combined efficiency and microstructural control advantages.

Key words: AZ91 magnesium alloy; constant-strain-rate extrusion; die geometry optimization; numerical simulation

1 Introduction

As the 21st century's most promising green engineering materials, magnesium alloys have become a cornerstone of global lightweighting strategies due to their low density and high specific strength[1–5]. Among these, AZ91 magnesium alloy is widely regarded as the most industrially promising material for its superior combination of strength and corrosion resistance. However, this alloy exhibits pronounced anisotropy in slip systems during room-temperature plastic deformation. The basal slip-dominated deformation mechanism results in inadequate formability under ambient conditions, significantly limiting its use in precision structural components[6–7].

Current research primarily focuses on two technological pathways: alloying modification and severe plastic deformation (SPD) [8]. In alloying modification, rare-earth elements (Nd, Gd, Y, etc) effectively weaken the basal texture and activate non-basal slip systems[9–12]. However, excessive rare-earth additions cause grain-boundary segregation and discontinuous precipitates, leading to strength-ductility trade-offs. Combined with resource scarcity and high costs, these limitations restrict industrial scalability[13–16].

In contrast, SPD offers unique advantages through grain refinement and texture control via intense plastic deformation, making it particularly suitable for low-ductility magnesium alloys[17]. The extrusion forming process, leveraging its

Received date: October 24, 2025
Foundation item: Key Research and Development Program of Shaanxi Province, China (S2024-YF-YBGY-1423); Xi'an Polytechnic University Graduate Student Innovation Fund (chx2025010)
Corresponding author: Cheng Xiaole, Ph. D., Professor, School of Mechanical and Electrical Engineering, Xi'an Polytechnic University, Xi'an 710048, P. R. China, E-mail: chengxiaole@xpu.edu.cn

inherent triaxial compressive stress field, effectively suppresses crack initiation[18], has become the cornerstone technology for strengthening magnesium alloys. This technique achieves exceptional process efficiency while enabling customization of diverse product morphologies.

In extrusion technology, backward extrusion exhibits superior triaxial compressive stress characteristics, making it widely applicable to tube and rod manufacturing. The recently developed rotary backward extrusion (RBE) introduces circumferential shear components, achieving a 40% improvement in equivalent strain homogeneity and a 15% increase in hardness for cup-shaped components[19–20]. However, studies indicate that both conventional backward extrusion (CBE) and RBE fundamentally lack active control over strain-rate fields[21].

The strain-rate sensitivity inherently poses two interrelated challenges in extrusion processes[22–23]. First, strain-rate gradients induce spatial heterogeneity in dynamic recrystallization and grain refinement, as shown by Chalay-Amoly et al[24], who identified microstructural inconsistencies in backward-extruded components using crystallographic analysis. This phenomenon is mechanistically similar to rate-dependent grain-boundary sliding observed in equal-channel angular pressing[25]. Simultaneously, localized high-strain-rate regions, particularly at die contact surfaces, trigger dynamic recovery and partial melting due to thermal transients from plastic work. These thermomechanical interactions exacerbate texture variations and promote the initiation of surface cracks, fundamentally limiting process stability and product consistency. Deka et al[26] confirmed that Mg-CeO_2 nanocomposites exhibit a 102.04% increase in strength but a 39.01% decrease in elongation as the strain rate increases from 0.0001 s^{-1} to 0.01 s^{-1} at 473 K. Shou et al[27] further revealed a strong strain-rate dependence of material ductility. Although Chen et al[28] theoretically proposed that controlled strain rates could produce AZ80 Mg alloy tubes with homogeneous microstructures and mechanical properties, practical implementation strategies remain absent.

Current research on constant-strain-rate backward extrusion (CSR-BE) remains limited. Our previous work on the B4CP/6063Al composite showed that using a constant-strain-rate die instead of a traditional die reduced the maximum tensile stress by 28.5%, increased the billet temperature at the die exit by 0.6%, and improved metal flow uniformity by 44%, highlighting the advantages of CSR-BE[29]. Building on this foundation, we proposed the novel CSR-BE method. The CSR-BE process introduces three key advancements over CBE. First, the mathematically optimized die profile enables automatic stabilization of strain rate. Second, the gradual curvature transition minimizes abrupt changes in the direction of material flow. Third, effective management of hydrostatic pressure gradients decouples strain-rate control from friction effects.

By integrating theoretical analysis with numerical simulations, the investigation elucidates the mechanism by which the stress state of AZ91 magnesium alloy is modulated under CSR-BE conditions. The process demonstrates dual improvements in extrudate mechanical properties and microstructural homogeneity, enabling continuous, industrial-scale production of isotropic magnesium alloy rods. These findings establish theoretical foundations for the extrusion forming of high-strength, high-ductility magnesium alloys and significantly expand their potential industrial applications.

2 Theoretical Foundation

The upper bound method requires the extrusion process to satisfy two fundamental conditions: the axisymmetric condition and the volume-conservation condition. The axisymmetric condition requires the billet to maintain a circular cross-section and to deform symmetrically about the central (z) axis. The volume conservation condition derives from the upper bound method's requirement for a kinematically admissible velocity field, specifically enforcing uniform velocity distributions in both the unextruded and extruded zones. This velocity field must simultaneously satisfy the volume conservation condition and the prescribed boundary constraints throughout the deformation zone.

2.1 CSR-BE

Within the unextruded zone, the billet maintains an initial velocity v_0. Upon entering the extruded zone through the die, the material flow accelerates, ultimately reaching the outlet velocity v_1. This velocity transition arises from the volume-conservation condition, yielding the continuity equation $A_0v_0= A_1v_1$, which governs the relationship between cross-sectional area and velocity.

Given the area ratio $\lambda = A_0/A_1$, the velocity relationship simplifies to $v_1 = \lambda v_0$. This proportionality implies a linearly increasing axial velocity field within the extruded zone, expressed as $v(x) \propto x$, where the material's axial velocity (v_x) demonstrates a strictly linear dependence on axial position, as shown in Eq.(1):

$$v_x(x) = v_0 + \frac{(v_1 - v_0)x}{L} = v_0\left[1 + (\lambda - 1)\frac{x}{L}\right] \tag{1}$$

where $v_x(x)$ is the axial velocity distribution function (mm/s); v_0 is the inlet velocity (mm/s); v_1 is the outlet velocity (mm/s); x is the transverse coordinate (mm); L is the length of the extrusion deformation zone (mm); λ is the extrusion ratio.

This relationship directly determines the axial strain rate (ε_x), expressed mathematically as:

$$\varepsilon_x = \frac{\partial v_x}{\partial x} = \frac{(\lambda - 1)v_0}{L} \tag{2}$$

Defining the process parameter $C \equiv (\lambda - 1)v_0/L$ ensures a constant axial strain rate. The volume conservation conditions impose a strain-rate compatibility constraint:

$$\varepsilon_x + \varepsilon_r + \varepsilon_\theta = 0 \tag{3}$$

where ε_θ refers to circumferential strain rate and ε_r refers to radial strain rate. Under axisymmetric deformation, the equivalence between ε_θ and ε_r arises from geometric constraints, yielding the fundamental strain rate relationship:

$$\varepsilon_r = \varepsilon_\theta = -\frac{\varepsilon_x}{2} = -\frac{C}{2} \tag{4}$$

where C is the constant axial strain rate (s^{-1}).

This derivation consequently establishes a constant radial strain rate. The equivalent strain rate $\dot{\varepsilon}_{eq}$ (s^{-1}) under these deformation conditions is defined by the von Mises criterion:

$$\dot{\varepsilon}_{eq} = \sqrt{\frac{2}{3}\left[\varepsilon_x^2 + 2\left(-\frac{\varepsilon_x}{2}\right]^2\right)} = \sqrt{\frac{2}{3} \times \frac{3\varepsilon_x^2}{2}} = \left|\varepsilon_x\right| \quad (5)$$

As shown in Eq.(5), the equivalent strain rate has a constant magnitude equal to the absolute value of the axial strain rate. This fundamental relationship demonstrates two critical characteristics: (1) strain rate uniformity throughout the extruded zone; (2) rigorous satisfaction of the requirements of CSR-BE method.

2.2 Die design

The axial coordinate system aligns the x-axis with the extrusion direction, with the die entrance (x=0) maintaining the initial radius a and the exit (x=L) attaining the reduced radius $b=a/\lambda$.

Mass conservation principles determine the axial velocity distribution:

$$v_x(x) = v_0\left(\frac{a}{r(x)}\right)^2 \quad (6)$$

This relationship directly links the velocity gradient to geometric confinement effects. Simultaneously enforcing the constant strain rate condition (Eq.(1) and Eq.(6)) yields the die profile:

$$r(x) = \frac{a}{\sqrt{1 + (\lambda - 1)\frac{x}{L}}} \quad (7)$$

where λ is the extrusion ratio; L is the die length.

3 Simulation Verification

3.1 Numerical verification

The extrusion process is simulated using DEFORM-3D finite element software. The billet material is AZ91 magnesium alloy, and the extrusion rod, die, and flat extrusion barrel are H13 steel. The chemical composition of the billet and the mechanical properties of H13 at room temperature are shown in Table 1 and Table 2.

During billet extrusion with this die, the cavity geometry ensures a constant strain rate throughout both the die-entry phase and steady-state extrusion, thereby maintaining uniformity of field variables throughout the deformation process. Given the axial symmetry of the die components, a quarter-section finite element model is developed and simulated in DEFORM-3D. The extrusion rod-pad assembly is simplified because the velocity profiles are identical during operation. The extrusion schematic is shown in Fig. 1. Compared to CBE, CSR-BE achieves precise strain-rate control through optimized reverse material flow and geometrically constrained die profiles. This approach effectively reduces frictional energy dissipation and lowers extrusion force, thereby overcoming the anisotropy limitations inherent in magnesium alloys.

Table 1 Chemical composition of AZ91 magnesium alloy (wt%)

Al	Zn	Mn	Si	Fe	Cu	Ni	Mg
9.3	0.63	0.32	0.05	0.003	0.021	0.001	Bal.

Table 2 Mechanical properties of H13 tool steel

Property	Yield Strength/MPa	Tensile Strength/MPa	Elongation/	Hardness, HRC
Value	1480	1620	8%–10%	52

For AZ91 magnesium alloy with a hexagonal close-packed (hcp) structure, slip-system activation strongly depends on deformation temperature. At room temperature, only the basal slip system is active. When the temperature exceeds 300 °C, the (1011) [1120] and (1010) [1120] slip systems begin to operate. Therefore, the billet temperature is set to 300 °C to activate basal slip and to enhance plastic deformation. The simulation boundary conditions are shown in Table 3.[30].

The constitutive behavior of AZ91 magnesium alloy is governed by the following relationship:

$$\dot{\varepsilon} = 2.8 \times 10^{12}[\sin(0.021\bar{\sigma})]^{5.578}\exp\left(-\frac{177}{8.314T}\right) \quad (8)$$

where $\dot{\varepsilon}$ is the strain rate, s^{-1}; $\bar{\sigma}$ is the effective stress, MPa; T is the absolute temperature, K. Heat transfer coefficients are specified as: 0.02 N/(s·mm·°C) among magnesium alloy billet, die, and ambient air and 11 N/(s·mm·°C) at billet-die interface.

3.2 Accuracy verification

The reliability and accuracy of the modeling and extrusion process are verified by comparing the extrusion force from the numerical simulation with theoretical upper-bound solutions. The upper-bound theorem is used to calculate the total power, which comprises the internal plastic-deformation power and the friction power. The plastic deformation power $W_{internal}$ in the extruded zone is expressed as:

$$W_{internal} = \int_V \sigma_y \dot{\varepsilon}_{eq} dV = \sigma_y \dot{\varepsilon}_{eq} V \quad (9)$$

where σ_y is the yield strength of AZ91 magnesium alloy, MPa;

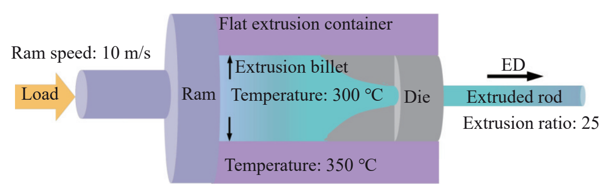

Fig.1 Schematic representation of CSR-BE

Table 3 Boundary conditions of numerical simulation

Parameter	Value
Extrusion speed, v/mm·s^{-1}	10
Initial billet temperature, T_0/°C	300
Friction coefficient	0.3
Initial temperature for die and ram/°C	350
Extrusion ratio of the extrusion zone	25
Total extrusion ratio	64

V is the total volume.

Since the equivalent strain rate $\dot{\varepsilon}$ remains constant, the domain of volumetric integration is the extruded zone, defined by the radial profile in Eq.(7) over the deformation zone ($0 \leqslant x \leqslant L$). The total volume V is therefore obtained by integration:

$$V = \int_0^L \pi r(x)^2 \mathrm{d}x = \frac{\pi a^2 L}{\lambda - 1} \ln\lambda \tag{10}$$

where a is the initial billet radius at extrusion inlet, mm; λ is the extrusion ratio; L is the length of the deformation zone, mm.

By combining Eq.(9) and Eq.(10), the internal deformation power is derived as:

$$W_{\text{internal}} = \sigma_y \dot{\varepsilon}_{\text{eq}} V = \sigma_y v_0 \pi a^2 \ln\lambda \tag{11}$$

Frictional power dissipation arises from shear stress at contact surfaces and relative sliding velocity. Based on the constant shear friction model, the frictional stress is formulated as proportional to the material's shear yield strength:

$$\tau = \frac{m\sigma_y}{\sqrt{3}} \tag{12}$$

where m is the friction factor ($0 \leqslant m \leqslant 1$).

Given that the frictional contact surface is primarily the die wall's cylindrical surface and that the relative sliding velocity is oriented along the axial direction, the following relationship holds:

$$W_{\text{friction}} = \int_0^L \tau v_x(x) 2\pi r(x) \mathrm{d}x \tag{13}$$

where W_{friction} is the frictional power (W). By substituting Eq.(1) and Eq.(7) into the power balance equation and performing the integration, the total extrusion force is derived as:

$$W_{\text{friction}} = \int_0^L \tau v_x(x) 2\pi r(x) \mathrm{d}x = \frac{4\pi\tau a v_0 L}{3(\lambda - 1)} \left(\lambda^{\frac{3}{2}} - 1\right) \tag{14}$$

The frictional component of the extrusion force is therefore determined as:

$$P_{\text{friction}} = \frac{W_{\text{friction}}}{v_0} = \frac{4\pi\tau a L}{3(\lambda - 1)} \left(\lambda^{\frac{3}{2}} - 1\right) \tag{15}$$

where P_{friction} is the frictional component of the extrusion force (N).

Substituting Eq.(12) into the above equation gives:

$$P_{\text{friction}} = \frac{4\pi m \sigma_y a L}{3\sqrt{3}(\lambda - 1)} \left(\lambda^{\frac{3}{2}} - 1\right) \tag{16}$$

The extrusion force is obtained from the total power balance equation:

$$W_{\text{total}} = W_{\text{internal}} + W_{\text{friction}} \tag{17}$$

Consequently, the extrusion force is determined as:

$$P = \sigma_y \pi a^2 \ln\lambda + \frac{4\pi m \sigma_y a L}{3\sqrt{3}(\lambda - 1)} \left(\lambda^{\frac{3}{2}} - 1\right) \tag{18}$$

The analytical solution predicts an extrusion force of 2.04 MN, while numerical simulations yield 2.05 MN, resulting in a relative error of 0.5%. This close agreement validates the computational accuracy of the finite element model for the CSR-BE methodology and confirms its predictive reliability within engineering tolerances.

Fig. 2 compares extrusion force profiles for CSR-BE and CBE processes. Under identical process parameters, the steady-state average loads are 2.24 MN for CBE and 2.05 MN for CSR-BE. CSR-BE process achieves a 9.3% reduction in extrusion force by optimizing strain-rate control. This reduction stems from the strain-rate sensitivity of the flow stress of the magnesium alloy. CSR-BE method maintains homogeneous deformation rates, thereby reducing overall flow stress and deformation resistance. The optimized die profile with gradual curvature transitions eliminates abrupt variations in interfacial contact, effectively suppressing friction-induced dead zones. This innovative design eliminates localized stress concentrations and energy-dissipation mechanisms prevalent in conventional extrusion. This comparative analysis confirms that CSR-BE process achieves a 9.3% reduction in extrusion force and demonstrates greater industrial viability than traditional backward extrusion under equivalent conditions.

4 Results and Discussion

4.1 Comparison of extrusion outlet uniformity

Assessing the efficacy of the extrusion process requires a multidimensional analysis of three governing physical fields: material flow velocity, stress distribution, and thermal gradients. Crucially, the homogeneity of the velocity field at the extrusion outlet is a key determinant of mechanical performance. Non-uniform flow velocity in metal extrusion induces significant mechanical anisotropy through heterogeneous stress partitioning and strain-energy accumulation, ultimately degrading tensile-strength consistency and yielding stability in extruded materials. This study implements nodal tracking analysis to quantitatively evaluate extrusion outlet homogeneity. Equidistant nodal points are selected along the horizontal axis of the outlet cross-section, enabling systematic observation of spatial variations between the billet core region and peripheral zones. The uniformity metric (S) is rigorously defined through variance analysis of field variables:

$$S = \frac{\sum_{i=1}^{n} (x_i - \bar{x})^2}{n - 1} \tag{19}$$

where x_i represents the nodal parameter value, $\bar{x}$ denotes the average value of the field variable across all nodes, and n

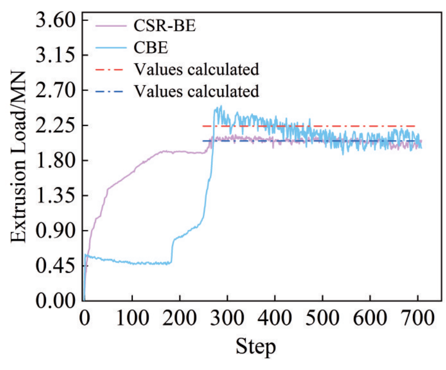

Fig.2 Extrusion force comparison between CSR-BE and CBE

indicates the number of monitored nodes. This statistical approach objectively characterizes heterogeneity in the field distribution while providing a scalar quantification of outlet uniformity.

Fig. 3a illustrates the nodal distribution characteristics of both CSR-BE and CBE. Fig. 3b shows distinct flow velocity characteristics between CSR-BE and CBE. In CSR-BE, nodal flow velocity curves remain nearly linear, with only minor velocity reductions at nodes 9–10 near the extrusion cylinder. In contrast, CBE exhibits abrupt deterioration in flow velocity beyond node 7, particularly near the cylinder interface. This behavior is attributed to elevated frictional power dissipation in conventional extrusion, which substantially impairs billet flow consistency, corroborating prior bulk flow analyses. Both processes show similar upward trends in equivalent stress (Fig. 3c) and outlet temperature (Fig. 3d). However, CSR-BE shows superior uniformity in strain distribution, with a 15.2% lower standard deviation than CBE, as quantified in Table 4.

CSR-BE process demonstrates superior material processing uniformity compared to CBE. CSR-BE achieves an average flow velocity of 243.7 mm/s with a variance of 0.16 mm/s, whereas CBE yields 230.4 mm/s with a variance of 426.9 mm/s, corresponding to a 99.96% improvement in flow uniformity. This enhanced homogeneity mitigates disparities in dislocation energy storage and promotes uniform fine-grain formation. Furthermore, CSR-BE exhibits an average residual stress of 42.75 MPa versus CBE's 43.64 MPa, representing an 85.2% improvement in stress uniformity. This advancement optimizes material anisotropy indices and refines grain-structure distributions. Although both processes exhibit comparable mean exit temperatures, CSR-BE reduces the variance of the temperature distribution by 81.6%, effectively suppressing localized abnormal grain growth.

This analysis confirms that CSR-BE methodology provides a theoretical framework for manufacturing high-performance magnesium alloys by synchronizing the optimization of flow-velocity fields, stress distributions, and thermal gradients. This multi-field homogenization mechanism ensures billet-property stability while effectively suppressing defect formation.

Prior research underscores the critical relationship between extrusion uniformity and material properties. As demonstrated by Che et al[31], enhanced deformation homogeneity directly improves dynamic recrystallization and mechanical performance, a principle foundational to the development of CSR-BE process. Although their work focused on RBE, the key takeaway, namely that uniformity-driven microstructure refinement increases recrystallization fractions by 72.6% and reduces hardness variations by 60%, validates the mechanistic

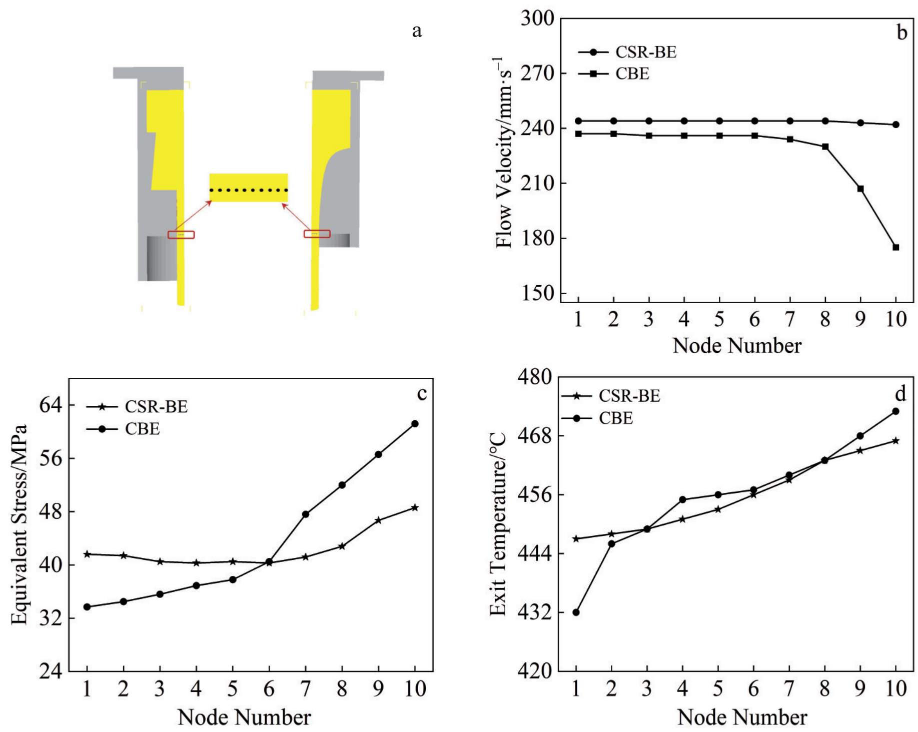

Fig.3 Nodal arrangement for material flow tracking (a); node flow velocity (b); node equivalent stress (c); node exit temperature (d)

Table 4 Comparison of extrusion uniformity between CSR-BE and CBE

Parameter	Mean		Variance		Uniformity improvement/%
	CSR-BE	CBE	CSR-BE	CBE	
Flow velocity/mm·s^{-1}	243.7	230.4	0.16	426.9	99.96
Equivalent stress/MPa	42.75	43.64	14.73	99.81	85.2
Exit temperature/°C	455.8	455.9	25.08	136.1	81.6

rationale behind our strain-rate control approach. Recrystallization ratios were quantified using an optical microscope and ImageJ thresholding; equiaxed grains meeting two criteria (aspect ratio <1.5 and boundary contrast threshold >80%) were classified as recrystallized zones. This comparative evidence from alternative extrusion methods reinforces the need for deformation homogeneity as a universal quality metric, thereby justifying our focus on strain-rate stabilization in CSR-BE. The microstructural improvements achieved through uniformity optimization in RBE (Fig.4a–4b) and the corresponding hardness consistency enhancements (Fig. 4c) serve as empirical benchmarks, confirming that the deformation homogeneity targeted by CSR-BE fundamentally determines extrudate quality. By transitioning from RBE's rotational shear to CSR-BE's strain-rate control, this study advances a more direct and energy-efficient pathway to achieving isotropic properties in magnesium alloys.

4.2 Stress distribution

During extrusion, the material undergoes plastic deformation under a triaxial compressive stress state in the deformation zone. The stress distribution critically governs extrudate uniformity, as localized tensile strain synergy that exceeds the material's fracture toughness initiates crack propagation and structural defects. Consequently, the magnitude and homogeneity of the stress fields within the deformation zone remain pivotal quality metrics for extruded components.

Both processes exhibit stress concentrations at the billet-plug contact interface, die entry, and die exit regions. However, CSR-BE process demonstrates superior stress distribution characteristics (Fig. 5a): it develops larger low-stress zones with gradual stress gradients in the deformation zone, while maintaining consistently lower equivalent stress values than CBE. Notably, CBE displays a distinct "low-high-low" stress distribution pattern across non-concentrated regions (Fig.5b). The stress concentration on the outer surface of the billet-plug contact is mainly due to the demarcation between the rigid and plastic zones, the sudden increase in shear stress on the contact surface between the pusher and the billet, and the transient change of the billet from rest to motion, which exacerbates plastic flow resistance. The stress state in the extruded zone is analyzed using slip-line theory. Slip-line theory can describe the stress state in the plastic zone and identify potential stress-concentration areas.

The stress state of the billet during CSR-BE process is

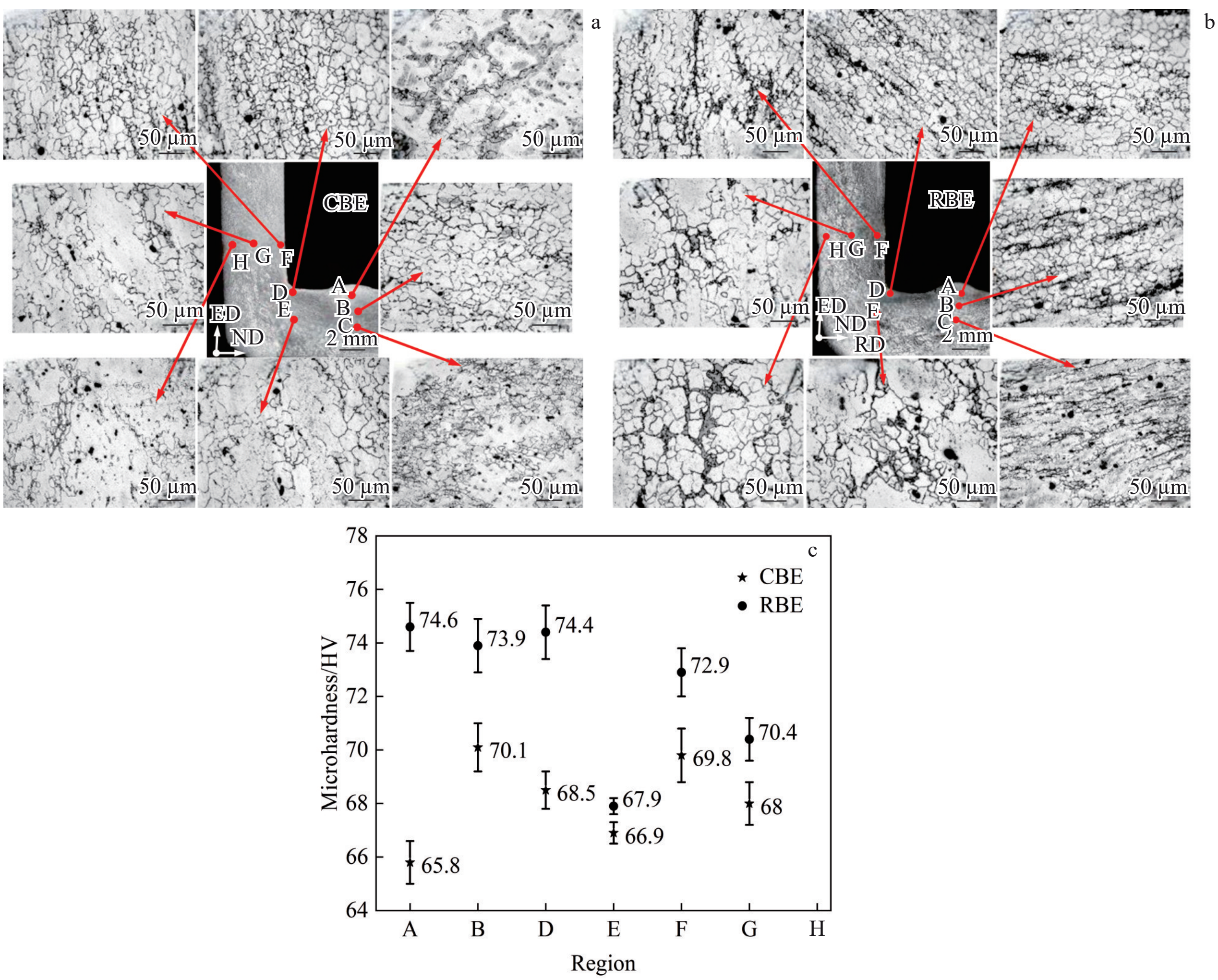

Fig.4 Comparison between CBE and RBE: (a–b) optical microstructures of the sample; (c) microhardness distribution

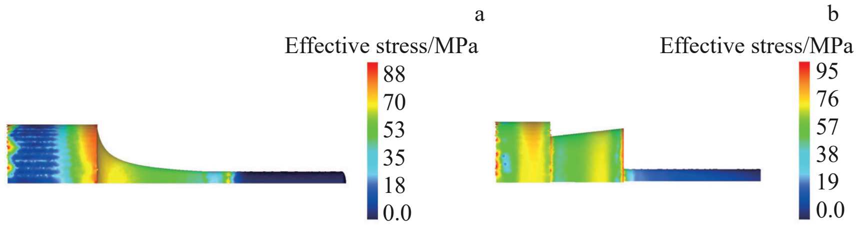

Fig.5 Comparative analysis of stress cloud maps between CSR-BE (a) and CBE (b)

analyzed using mechanical equilibrium conditions. Given the axisymmetric nature of the extrusion process, a cylindrical coordinate system is adopted, along with the corresponding slip-line field configuration. Fig.6 illustrates the characteristic stress distribution, where the shear stress components satisfy $\tau_{\theta r} = \tau_{\theta z} = 0$, and σ_θ acts as a principal stress. The governing stress equilibrium equations are expressed as:

$$\begin{cases} \sigma_r = -p_m - K\sin 2\phi \\ \sigma_z = -p_m + K\sin 2\phi \\ \tau_{rz} = K\cos 2\phi \\ \sigma_\theta = -p_m + \alpha K \end{cases} \tag{20}$$

where p_m is the hydrostatic pressure component; $K = \sigma_y/\sqrt{3}$; ϕ is the angle between the slip-line's tangent and the coordinate axis; α is the annular stress coefficient (determined by the material's anisotropy or deformation constraints, and assumed to be 0 for isotropy).

The stress state under axisymmetric conditions is governed by the following equilibrium equations:

$$\begin{aligned} &\frac{\partial \sigma_r}{\partial r} + \frac{\partial \tau_{rz}}{\partial z} + \frac{\sigma_r - \sigma_\theta}{r} = 0 \\ &\frac{\partial \tau_{rz}}{\partial r} + \frac{\partial \sigma_z}{\partial z} + \frac{\tau_{rz}}{r} = 0 \end{aligned} \tag{21}$$

Combining Eq. (20) and Eq. (21) yields the stress relationship for axisymmetric extrusion:

$$\begin{cases} \dfrac{\partial p_m}{\partial r} - K\dfrac{\partial \sin 2\phi}{\partial r} - \dfrac{K}{r}\sin 2\phi + K\dfrac{\partial \cos 2\phi}{\partial z} = 0 \\ K\dfrac{\partial \cos 2\phi}{\partial r} + \dfrac{K}{r}\cos 2\phi - \dfrac{\partial p_m}{\partial z} + K\dfrac{\partial \sin 2\phi}{\partial z} = 0 \end{cases} \tag{22}$$

To simplify the solution of the above equation, ϕ can be kept constant; thus, the differential term in Eq. (22) with respect to the angle of ϕ is zero, and the equation can be simplified as:

$$\begin{cases} \dfrac{\partial p_m}{\partial r} + \dfrac{K}{r}\sin 2\phi = 0 \\ \dfrac{\partial p_m}{\partial z} - \dfrac{K}{r}\cos 2\phi = 0 \end{cases} \tag{23}$$

In axisymmetric problems, the radial and axial stress components may influence the direction of the slip-line. There is friction between the constant-strain-rate die and the blank, and the shear stress at the contact surface at the inlet satisfies the friction condition at the die surface:

$$\tau_{rz} = m\tau_y \tag{24}$$

where τ_y is the shear yield strength, based on the given stress components:

$$\tau_{rz} = K\cos 2\phi \tag{25}$$

The material behavior follows the Tresca yield criterion with the yield shear stress defined as $K = \tau_y = 34.64$ MPa.

From the associative Eq.(22) and Eq.(23), the friction factor m=0.3 is known for the CSR-BE method, and the initial angle $\phi(0)\approx 36.27°$ is obtained. Along the streamline direction (dz=dx), the slip-line angle $\phi(x)$ satisfies:

$$\frac{\partial \phi}{\partial x} = \frac{\sin 2\phi}{r}\frac{\mathrm{d}r}{\mathrm{d}x} - \frac{\cos 2\phi}{r} \tag{26}$$

Solving Eq. (26) yields the extruded exit angle ϕ (150) ≈ 11.3° and the midpoint of the extruded zone $\phi(75)\approx 25°$.

During CBE, the extruded zone is curved:

$$r(x) = \begin{cases} 80 & 0 \leqslant x < 50 \\ 0.1x + 55 & 50 \leqslant x \leqslant 150 \end{cases} \tag{27}$$

Letting the above equation be associated with Eq.(19), the material satisfies the Tresca yield criterion, which means that the slip-line angle $\phi(x)$ satisfies CBE:

$$\frac{\mathrm{d}\phi}{\mathrm{d}x} = \frac{\sin 2\phi}{r(x)}\left(1 + \frac{\mathrm{d}r/\mathrm{d}x}{\tan 2\phi}\right) \tag{28}$$

Therefore, $\phi(0)\approx 36.27°$, the angle of extruded zone $\phi(150)\approx$ 17.1°, and the midpoint of extruded zone $\phi(75)\approx 35.2°$.

The coupled solution of Eq.(20) and Eq.(23) systematically determines the stress distribution throughout the extrusion zone. Table 5 quantifies stress magnitudes at critical deformation locations, thereby validating the theoretical framework for CSR-BE process analysis.

Both extrusions are based on the backward extrusion process, which applies slip-line theory to analyze material

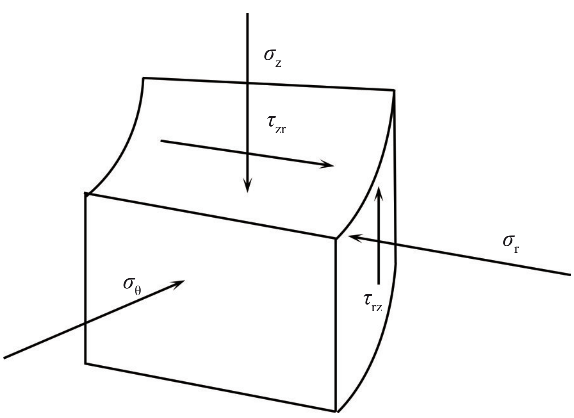

Fig.6 Axisymmetric stress state analysis in CSR-BE process

Table 5 Quantitative stress distribution analysis in extrusion zones

Location	Process type	$\phi(x)$	p_m/MPa	σ_r/MPa	σ_z/MPa	τ_{rz}/MPa
Inlet	CSR-BE	36.27°	p_0–33.0	–p_0+0.1	–p_0+65.9	10.39
	CBE	45°	p_0–34.64	–p_0+34.74	–p_0+100.5	34.64
Outlet	CSR-BE	11.3°	p_0+32	–p_0–35.5	–p_0–18.49	31.9
	CBE	17.1°	p_0+135	–p_0–105.0	–p_0–165.0	17.3
Core	CSR-BE	25°	p_0–26.6	–p_0–0.1	–p_0+53.3	22.2
	CBE	35.2°	p_0–29.9	–p_0+47.22	–p_0+12.58	30.0

flow and induces plastic deformation through hydrostatic-pressure gradients, with their stress components following the equation above. However, there are significant differences between the two in key parameters and process effectiveness. In CBE, the slip-line angle $\phi(x)$ decreases from 35.0° to 17.1° at the exit, resulting in a sudden change in material flow direction, a steep hydrostatic pressure gradient, and a sudden increase at the exit from p_m to p_0+135 MPa, resulting in a radial stress $\sigma_r=-p_0-105.0$ MPa, close to the material high-temperature yield limit, and a smaller superimposed shear stress τ_{rz}=17.3 MPa, which is prone to shear instability and induces surface cracks. In addition, the internal material flow is dominated by radial shear, and the core flow is slow, which makes it easy to form defects. In contrast, CSR-BE realizes a natural transition of flow direction through a continuous curve of $\phi(x)$ with a smooth hydrostatic pressure gradient, and the outlet p_m only increases to p_0+32 MPa, and inside the extruded zone, the slip-line direction angle $\phi(x)$ decreases from 36.27° at the inlet to 11.3° at the outlet, with $\sigma_r=-P_0-0.1$ MPa and $\sigma_z=-P_0+53.3$ MPa, indicating that the material flow mode transitions from radial shear to axial stretching and is accelerated by the hydrostatic pressure gradient-driven core material.

At the extrusion outlet, the axial stress $\sigma_z=-p_0-18.49$ MPa and the radial stress $\sigma_r=-p_0-35.5$ MPa, exhibiting a controlled differential stress gradient. This gradient-driven flow acceleration within the billet mitigates internal defects while keeping stress levels well below the material's yield limit, thereby preventing localized instability. The exit stress state is then verified using Mohr's circle, as shown in Fig.7. It satisfies the condition $\tau_{rz}^2+(\sigma_z+p_m)^2=K^2$, lies on the yield surface, and confirms that the theoretical model is self-consistent.

In summary, CSR-BE is better suited for complex cross-section molding of high-strength materials, thanks to its uniform stress distribution, controllable flow, and stability suppression. It is especially advantageous for manufacturing precision parts, where it balances efficiency and quality, delivering significant benefits.

4.3 Flow velocity

Fig. 8 shows the metal flow rate distribution at different stages of CSR-BE and CBE. During extrusion, friction at the billet-die interface reduces the flow velocity at the billet surface relative to the central region. This velocity difference causes only the central portion of the billet to effectively fill the die cavity, creating a distinct demarcation line at the contact interface. In CSR-BE, the flow demarcation boundary appears only during the final extrusion phase and occupies a minimal area within the surface layer (Fig. 8a). All material interior to this line exhibits unidirectional flow aligned with the extrusion axis. In contrast, CBE exhibits distinct flow characteristics (Fig. 8b), with the demarcation boundary forming in the bille's surface layer during early-stage extrusion. Subsequent processing stages show progressive inward migration of this interface (indicated by red trajectory markers), accompanied by intensifying flow stratification, a phenomenon detrimental to homogeneous billet formation. Compared with the corresponding extrusion stage, the flow velocity of CSR-BE is higher than that of CBE, indicating that the former exhibits a better extrusion effect and that its extrusion method is more conducive to billet plastic deformation.

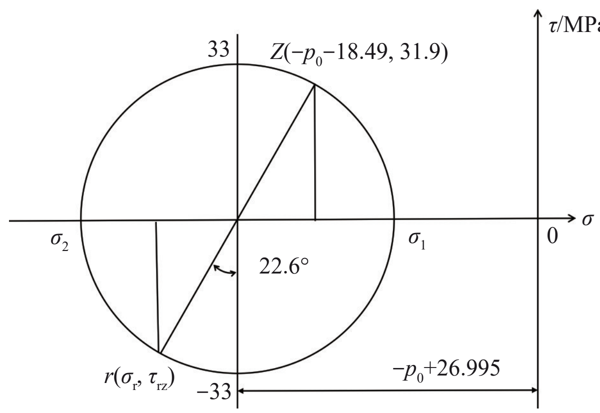

Fig.7 Mohr's circle analysis of stress state conformity

Fig. 9 presents velocity histograms for the extrusion processes. CSR-BE exhibits a maximum flow velocity of 290 mm/s and an average of 68.5 mm/s (Fig. 9a), whereas CBE shows 237 and 58.7 mm/s, respectively (Fig. 9b). This comparison indicates a 22.4% increase in maximum velocity and a 16.7% increase in average velocity for CSR-BE. CSR-BE maintains a constant strain rate by controlling the geometric deformation gradient through the die profile.

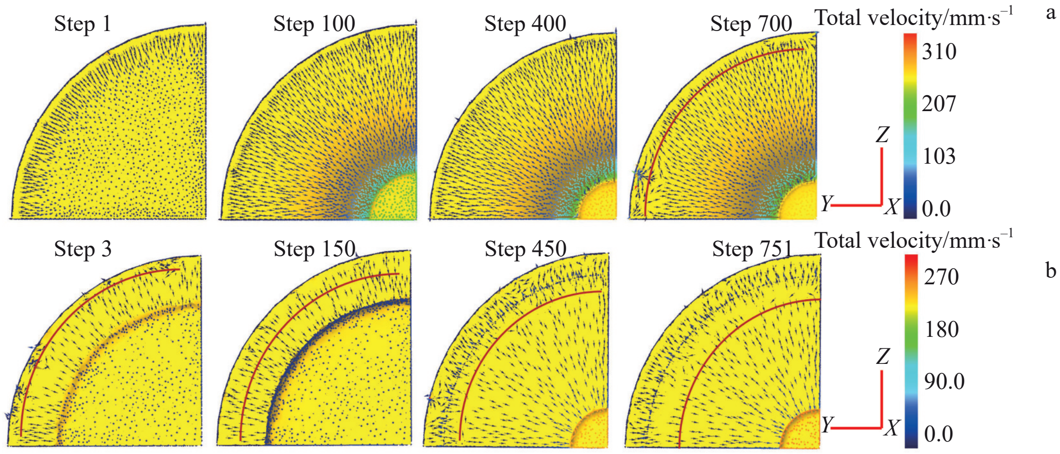

Fig.8 Flow velocity distribution comparison between CSR-BE (a) and CBE (b)

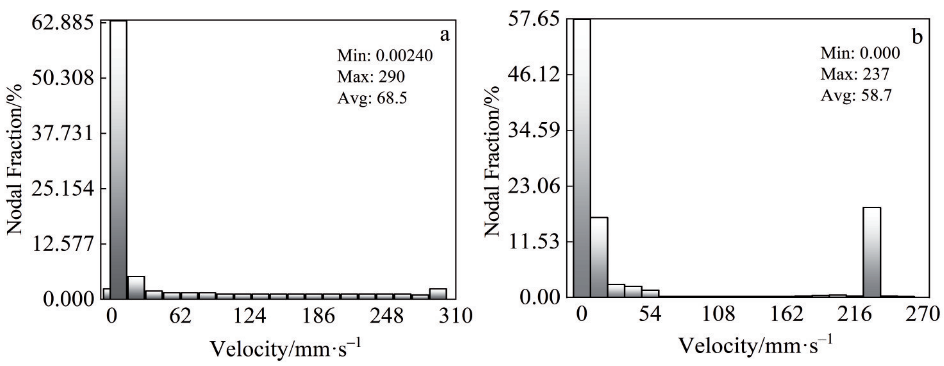

Fig.9 Flow velocity histogram comparison between CSR-BE (a) and CBE (b)

In contrast, CBE exhibits high peak friction power due to the nonlinear variation of $\dot{\varepsilon}_{eq}$, which inhibits the billet flow rate. CSR-BE also achieves a uniform stress field across the slip-line angle $\phi(x)$, avoiding the surge in flow resistance caused by the sudden change in local strain rate in CBE. The surface friction shear stress is uniformly distributed along the die surface. Therefore, the maximum and average flow rates of CSR-BE are higher than those of CBE.

Quantitative analysis of the flow rate for CSR-BE begins with the assumption that the material follows the modified Norton-Hoff constitutive equation:

$$\sigma_y = \sigma_0\left(1 + \frac{\dot{\varepsilon}_{eq}}{\dot{\varepsilon}_0}\right)^m \exp\left(-\frac{T-T_0}{T_m}\right) \tag{29}$$

where σ_0 is the high-temperature yield strength of AZ91 magnesium alloy, 50 MPa; $\dot{\varepsilon}_0$=0.1 s^{-1}; T_0 is the initial temperature, and T_m is the melting point of the magnesium alloy.

Considering the surface shear stress $\tau_{rz} = mK$, the friction power is converted into axial kinetic energy gain (Δv):

$$\Delta v = \frac{mK}{2\sigma_0} = 0.1039 \tag{30}$$

The dynamic recrystallization softening factor $\alpha(T)$ is introduced to account for the additional softening effect of dynamic recrystallization and to correct $\alpha(T)$. Thus, the maximum flow rate equation is established as:

$$v_z^{max} = \lambda v_0 \alpha(T)(1 + \Delta v) = 275.98\alpha(T) \tag{31}$$

where $\alpha(T)$ is the dynamic recrystallization softening factor and v_z^{max} is the maximum axial flow velocity (mm/s).

According to Fig. 8, the maximum flow velocity is 290 mm/s. Substituting into Eq.(31) yields $\alpha(T)$ = 1.12, so the equation for the maximum flow velocity is:

$$v_z^{max} = 1.236\lambda v_0 \tag{32}$$

5 Conclusions

1) CSR-BE is innovatively proposed and the corresponding die structure is designed. The die curve is $r(x) = a/\sqrt{1 + (\lambda-1)x/L}$, to achieve constant strain-rate control in the extruded zone, reducing the extrusion pressure by 9.3% compared with the traditional process. In addition, energy consumption is significantly reduced by eliminating the friction dead zone and strain-rate fluctuations.

2) The optimized CSR-BE method significantly enhances homogeneity in the extruded zone, demonstrating a 99.96% reductions in flow velocity variance, an 85.2% reduction in stress variance, and an 81.6% reduction in temperature-field variance at the exit region. These quantified improvements establish a theoretical framework for achieving isotropic characteristics in high-strength magnesium alloy products.

3) The interaction between die geometry and interfacial friction fundamentally alters material flow patterns. The slip-

line orientation angle decreases linearly from 36.27° at the die entrance to 11.3° at the extrusion outlet. This transition shifts the dominant deformation mechanism from radial shear to axial stretching flow. Concurrently, the gradual hydrostatic pressure gradient mitigates local stress concentrations, thereby preventing shear localization and the initiation of surface cracks.

4) CSR-BE method fundamentally enhances flow dynamics, yielding a 22.4% increase in maximum velocity and a 16.7% improvement in average velocity over conventional processes. This strain-rate stabilization eliminates abrupt local surges in resistance characteristic of CBE, thereby ensuring a uniform distribution of die-surface frictional shear stress along the deformation path.

References

1 Xu Q, Ma A, Li Y *et al. Journal of Magnesium and Alloys*[J], 2020, 8(1): 192

2 Song J F, She J, Chen D L *et al*. *Journal of Magnesium and Alloys*[J], 2020, 8(1): 1

3 Wang D, Jing Y, Gao Y *et al. Journal of Materials Research and Technology*[J], 2023, 27: 4430

4 Chai F, Ma Z, Han X *et al. Journal of Materials Research and Technology*[J], 2023, 27: 4644

5 Mo Y, Jiang F, Xu H *et al. Journal of Magnesium and Alloys*[J], 2024, 12(7): 2826

6 Ramalingam V V, Ramasamy P, Kovukkal M D *et al. Metals and Materials International*[J], 2020, 26: 409

7 Imandoust A, Barrett C D, Al-Samman T *et al. Journal of Materials Science*[J], 2017, 52: 1

8 Yu H, Park S H, You B S. *Materials Science and Engineering A*[J], 2014, 610: 445

9 Du P, Mei D, Furushima T *et al. Journal of Magnesium and Alloys*[J], 2022, 10(5): 1286

10 Zhang D, Pan H, Li J *et al. Materials Science and Engineering A*[J], 2022, 833: 142565

11 Xu Y, Li J, Qi M *et al. Materials Characterization*[J], 2022, 188: 111867

12 Zhai Y X, Hou X L, Yuan Z Z *et al. Rare Metal Materials and Engineering*[J], 2018, 47(5): 1341

13 Qin P F, Yang Q, He Y Y *et al. Rare Metals*[J], 2021, 40: 2956

14 Bian M, Huang X, Mabuchi M *et al. Journal of Alloys and Compounds*[J], 2020, 818: 152891

15 Li Y Q, Li F, Kang F W *et al. Journal of Alloys and Compounds*[J], 2023, 953: 170080

16 Ping L I, Xue K, Wang X *et al. Transactions of Nonferrous Metals Society of China*[J], 2014, 24(5): 1289

17 He R H, Wang H, Zhang Z *et al. Rare Metal Materials and Engineering*[J], 2023, 52(11): 3697

18 Masuda T, Horita Z. *Materials Transactions*[J], 2019, 60(7): 1104

19 Yan L, Zhang Z, Li G *et al. Journal of Alloys and Compounds*[J], 2021, 877: 160229

20 Che X, Wang Q, Dong B *et al. Journal of Magnesium and Alloys*[J], 2021, 9(5): 1677

21 Zheng J, Sheng F, Chen Z *et al. Journal of Alloys and Compounds*[J], 2025, 1010: 178278

22 Faraji G, Jafarzadeh H, Jeong H J *et al. Materials & Design*[J], 2012, 35: 251

23 Wang H, Lin M, Zhu M, Pan W *et al*. *Journal of Magnetism and Magnetic Materials*[J], 2012, 324: 1791

24 Chalay-Amoly A, Zarei-Hanzaki A, Changizian P *et al. Materials & Design*[J], 2013, 47: 820

25 Cui L, Shao S, Wang H *et al. Processes*[J], 2022, 10(11): 2181

26 Deka S, Mozafari F, Mallick A. *Composites Part A: Applied Science and Manufacturing*[J], 2024, 177: 107936

27 Shou H G, Zheng J, He L Y *et al. Acta Materialia*[J], 2025, 284: 120633

28 Chen Z, Zheng J, Zhang Z *et al. Journal of Materials Processing Technology*[J], 2023, 319: 118081

29 Cheng X L, Yuan J C, Yin J *et al. Journal of Plasticity Engineering*[J], 2020, 27(2): 37

30 Gong Y, He J G, Wen J B *et al. Rare Metal Materials and Engineering*[J], 2023, 52(2): 508

31 Che X, Wang Q, Dong B *et al. Journal of Magnesium and Alloys*[J], 2021, 9(5): 1677

AZ91镁合金等应变速率反向挤压新工艺

张鹏涛[1]，成小乐[1]，任玺君[2]，张　敏[1]，边承浩[1]，孙　戬[1]，赵小惠[1]，苏振华[3]

(1. 西安工程大学 机电工程学院，陕西 西安 710048)

(2. 西安西材三川智能制造有限公司，陕西 西安 710600)

(3. 中国重型机械研究院股份公司，陕西 西安 710018)

摘　要：针对AZ91镁合金室温延展性差和各向异性显著的问题，提出一种通过协同调控模具曲率和应变速率来提升变形均匀性的恒应变速率反挤压（CSR-BE）工艺。该方法结合轴对称滑移线理论和体积恒定原理建立模具型面方程，实现全流程应变速率精确控制。DEFORM-3D模拟表明，相较于传统反挤压，CSR-BE工艺使挤压力降低9.3%，并显著改善变形均匀性：出口区流速方差降低99.96%，应力场差异下降85.2%，温度分布波动减少81.6%。机理分析表明，优化模具结构使材料流动模式从径向剪切主导转变为轴向拉伸主导，滑移线取向角从入口处的36.27°线性递减至出口处的11.3°。梯度化静水压力分布有效缓解局部应力集中，同时消除摩擦死区并抑制应变速率波动。基于理论基础的应力与流速定量计算证实，该方法解决了传统工艺的微观组织异质性问题。CSR-BE工艺建立了具有理论依据的镁合金棒材高效制备策略，通过协同增效的工艺控制和微观调控优势，在提升各向同性的同时展现出工业化应用潜力。

关键词：AZ91镁合金；等应变速率挤压；模具设计；数值模拟

作者简介：张鹏涛，男，1999年生，硕士，西安工程大学机电工程学院，陕西　西安　710048，E-mail：15686992298@163.com